applied sciences

MDPI

Article

Buckling Analysis of CNTRC Curved Sandwich Nanobeams in Thermal Environment

Ahmed Amine Daikh [1], Mohammed Sid Ahmed Houari [1], Behrouz Karami [2], Mohamed A. Eltaher [3,4], Rossana Dimitri [5] and Francesco Tornabene [5,*]

1 Laboratoire d'Etude des Structures et de Mécanique des Matériaux, Département de Génie Civil, Faculté des Sciences et de la Technologie, Université Mustapha Stambouli, B.P. 305, Mascara 29000, Algeria; ahmed.daikh@univ-sba.dz (A.A.D.); ms.houari@univ-mascara.dz (M.S.A.H.)
2 Department of Mechanical Engineering, Marvdasht Branch, Islamic Azad University, Marvdasht 15914, Iran; behrouz.karami@miau.ac.ir
3 Faculty of Engineering, Mechanical Engineering Department, King Abdulaziz University, P.O. Box 80204, Jeddah 21589, Saudi Arabia; meltaher@kau.edu.sa
4 Faculty of Engineering, Mechanical Design and Production Department, Zagazig University, P.O. Box 44519, Zagazig 44519, Egypt
5 Department of Innovation Engineering, Università del Salento, 73100 Lecce, Italy; rossana.dimitri@unisalento.it
* Correspondence: francesco.tornabene@unisalento.it

Abstract: This paper presents a mathematical continuum model to investigate the static stability buckling of cross-ply single-walled (SW) carbon nanotube reinforced composite (CNTRC) curved sandwich nanobeams in thermal environment, based on a novel quasi-3D higher-order shear deformation theory. The study considers possible nano-scale size effects in agreement with a nonlocal strain gradient theory, including a higher-order nonlocal parameter (material scale) and gradient length scale (size scale), to account for size-dependent properties. Several types of reinforcement material distributions are assumed, namely a uniform distribution (UD) as well as X- and O- functionally graded (FG) distributions. The material properties are also assumed to be temperature-dependent in agreement with the Touloukian principle. The problem is solved in closed form by applying the Galerkin method, where a numerical study is performed systematically to validate the proposed model, and check for the effects of several factors on the buckling response of CNTRC curved sandwich nanobeams, including the reinforcement material distributions, boundary conditions, length scale and nonlocal parameters, together with some geometry properties, such as the opening angle and slenderness ratio. The proposed model is verified to be an effective theoretical tool to treat the thermal buckling response of curved CNTRC sandwich nanobeams, ranging from macroscale to nanoscale, whose examples could be of great interest for the design of many nanostructural components in different engineering applications.

Keywords: curved sandwich nanobeams; nonlocal strain gradient theory; quasi-3D higher-order shear theory; thermal-buckling

Citation: Daikh, A.A.; Houari, M.S.A.; Karami, B.; Eltaher, M.A.; Dimitri, R.; Tornabene, F. Buckling Analysis of CNTRC Curved Sandwich Nanobeams in Thermal Environment. *Appl. Sci.* **2021**, *11*, 3250. https://doi.org/10.3390/app11073250

Academic Editor: Antonio Di Bartolomeo

Received: 27 February 2021
Accepted: 31 March 2021
Published: 5 April 2021

1. Introduction

Multilayered composites are widely used in various engineering structures, ranging from macroscale (i.e., aircraft, submarines, space-station structures, etc.) to nanoscale (nano-sensors, nano-actuators, nano-gears, and micro/nano-electro-mechanical systems (MEMS/NEMS), due to the high stiffness and strength-to-weight ratios caused by fiber reinforcements. In the recent literature, reinforcements based on carbon nanotubes (CNTs) have been largely applied in lieu of conventional fibers due to their excellent properties in order to improve the mechanical, electrical, and thermal properties of composite structures. In [1,2], for example, different molecular dynamic simulations have been successfully applied by the authors to exploit the elastic moduli of polymer–CNT composites embedded

in polymeric matrices. Fidelus et al. [3] examined the thermo-mechanical properties of different epoxy-based nanocomposites with randomly oriented single-walled (SW) and multi-walled (MW) CNTs. Moreover, Shen [4] investigated the nonlinear bending behavior of FG nanocomposite plates reinforced by SWCNTs subjected to a transverse uniform or sinusoidal load in a thermal environment using two different distribution functions. A nonlocal strain gradient theory was also proposed by Lim et al. [5] to study a wave propagation in macro and nanobeam structures for the first time. Wu and Kitipornchai [6] investigated the free vibration and elastic buckling of sandwich beams with a stiff core and functionally graded (FG)-CNTRC face sheets in a Timoshenko beam theoretical framework. Among coupled thermo-mechanical problems, Eltaher et al. [7] investigated the influence of a thermal loading and shear force on the nonlocal buckling response of nanobeams via higher-order shear deformation Eringen beam theories. Similarly, Ebrahimi and Farazmandnia [8] investigated the thermo-mechanical vibration of sandwich FG-CNTRC beams within a Timoshenko-based beam approach; Sobhy and Zenkour [9] illustrated the influence of a magnetic field on the thermo-mechanical buckling and vibration response of FG-CNTRC nanobeams with a viscoelastic substrate. In line with the previous works, Daikh and Megueni [10] studied the thermal buckling of FG sandwich higher-order plates with material temperature-dependent properties under a nonlinear temperature rise; Arefi and Arani [11] combined a third-order shear deformation approach together with the nonlocal elasticity to study the static deflection of FG nanobeams under a coupled thermo-electro-magneto-mechanical environment. A novel refined shear theory was recently proposed by Bekhadda et al. [12] for the study of a gradation influence on the vibration and buckling behavior of FG beams with a power-law function by means of Fourier series. Medani et al. [13], instead, applied the first order shear deformation and energy principle to study the static and dynamic behavior of FG-CNT-reinforced porous sandwich plates. Arani et al. [14] later performed a thermo-electro-mechanical buckling study of FG-CNTRC sandwich nanobeams based on a nonlocal strain gradient elasticity theory and differential quadrature numerical procedure. More complicated double-curved sandwich panels were accounted by Nejati et al. [15], who analyzed the thermal vibration in presence of pre-strained shape memory alloy wires. Chaht et al. [16] analyzed the size-dependent static behavior of FG nanobeams, including the thickness stretching effect; whereas a nonlocal trigonometric shear deformation theory and nonlocal quasi-3D theory were proposed in [17,18], respectively, to treat FG nanobeams. An efficient alternative tool to handle nonlocalities within nanostructures is represented by the strain gradient theory, as successfully applied in [19,20] for the thermal snap-buckling and bending analysis of FG curved porous and non-porous nanobeams and in [21,22] for the buckling study of porous FG sandwich nanoplates resting on a Kerr foundation due to a heat conduction. A theoretical formulation based on a Reddy shear deformation theory, has been also proposed in the recent work by Daikh et al. [23] to study the buckling and vibration of FG-CNTRC-laminated nanoplates in thermal environment, with promising results for engineering applications. Furthermore, Daikh et al. [24] investigated the thermal buckling response of FG sandwich beams under a power-law (P-FGM) or sigmoid (SFGM) variation. Further attempts of combining higher order theories and nonlocal approaches in a unified context, can be found in [25–28] to predict the influence of an axial in-plane load function on the critical buckling load and mode shape of composite beam members, also in presence of porosities. During fabrication, structural members can exhibit an initial curved shape as possible imperfection related to iterative heating and cooling processes. Many MEMS devices employ curved structures as well [29]. The initial curvature of a beam structure can be a source of difficulty in developing the constitutive relations, as verified by Emam et al. [30], who illustrated the possible effects of curvatures and imperfections on the post-buckling and free vibration response of multilayer nonlocal prestressed nanobeams. Shi et al. [31] also studied the effect of nanotube waviness and agglomeration on the elastic property of CNT-reinforced composites. A further systematic study was performed by Khater et al. [32], who investigated the impact of the surface energy and thermal loading on the

static stability of curved nanowires, modeled as curved Euler-Bernoulli beams, accounting for both the von Karman and axial strain field. Among more sophisticated shell models, a valuable comparison between different higher-order formulations was proposed in [33–35] for the static analysis of multilayered composite and sandwich plates and shells, both from a theoretical and computational perspective. Mohamed et al. [36] later proposed a differential quadrature method to study the nonlinear free and forced vibrations of buckled curved beams resting on nonlinear elastic foundations. A further attempt of combining the nonlocal strain gradient and higher-order shell theories was conducted by Karami et al. [37] for a wave dispersion study in anisotropic doubly-curved nanoshells, as well as in [38–41] for FG-CNTRC curved nanobeams also in coupled piezoelectric conditions. In another work, Arefi et al. [42] predicted the static deflection and stress field of curved FG-CNTRC nonlocal Timoshenko nanobeams resting on an elastic foundation under four different distribution patterns of CNTs throughout the thickness direction. Eltaher et al. [43] also presented the influence of periodic and/or nonperiodic imperfections on the buckling, post-buckling and dynamic response of curved beams resting on nonlinear elastic foundations by means of high-performing numerical differential-integral quadrature methods (DIQMs). Malikan et al. [44] developed a theoretical model to study the dynamics of non-cylindrical curved viscoelastic SWCNTs by applying a second gradient theory of stress-strain, whereas Mohamed et al. [45] used an energy equivalent model to study the post-buckling response of imperfect CNTs resting on a nonlinear elastic foundation, including mid-plane stretching and nanoscale effects. Among the most recent works on the topic, Van Tham et al. [46] developed a novel four-variable refined shell theory to study the free vibration of multi-layered FG-CNTRC doubly curved shallow shell panels; Dindarloo et al. [47] exploited the strain-driven nonlocal integral theory to study the bending response of isotropic doubly curved high-order shear deformation nanoshells under a combined assumption of exponential and trigonometric shape functions. Furthermore, Eltaher and Mohamed [48] exploited the nonlinear stability and vibration of imperfect CNTs modeled as Euler-Bernoulli beams with a mid-plane stretching, while in [49–51], the authors studied the free and forced vibration and the dispersion behavior of elastic waves of doubly-curved nonlocal strain gradient theory nanoshells in conjunction with a higher-order shear deformation shell theory. Based on the available literature, however, the influence of a material scale, size scale, and graduation distribution functions on the thermal static stability of curved sandwich nanobeams with temperature-dependent material seems to be generally lacking. To this end, the present paper aims at providing a closed-form solution to the problem, for different boundary conditions, that could be useful as theoretical benchmark for different computational studies and engineering design applications. The paper is organized as follows. In Section 2, the theoretical formulation of curved sandwich CNTRC nanobeams is reviewed, including the kinematic field, relations and constitutive equations. Section 3 illustrates the governing equilibrium equation of curved sandwich beams in a classical and nonclassical domain, while discussing about different thermal field distributions and temperature-dependent properties of materials. Section 4 presents the analytical solutions of the problem for different boundary conditions, whose comparative study is performed systematically and discussed in Section 5. Finally, in Section 6, conclusions are drawn together with possible future research directions.

2. Theoretical Formulation

2.1. Geometric and Mechanical Properties

A symmetric cross-ply single-walled carbon nanotube reinforced composite (CNTRC) curved sandwich beam of length L, thickness h, and radius of curvature R is considered, as shown in Figure 1. Different volume fraction distributions of CNTs are here assumed throughout the thickness (see Figure 2), in agreement with the following relations [22]:

- UD (Uniformly-Distributed) CNTRC multilayered nanobeam:

$$V_{cnt} = V_{cnt}^{*} \tag{1}$$

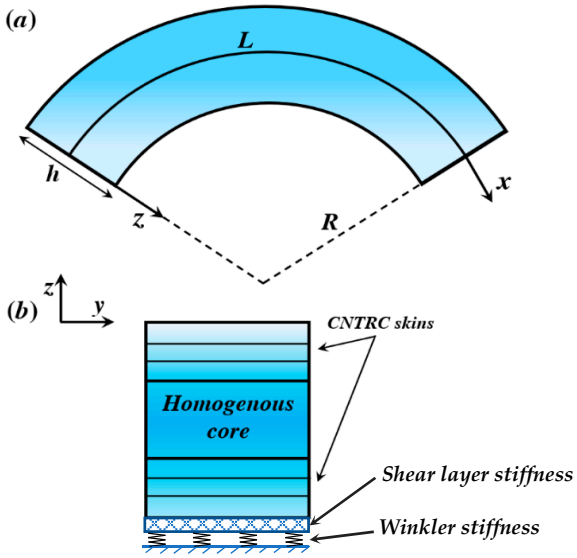

Figure 1. Geometry of a carbon nanotube reinforced composite (CNTRC) curved sandwich beam: (**a**) geometric parameters of the curved beam, (**b**) cross-section of the curved beam.

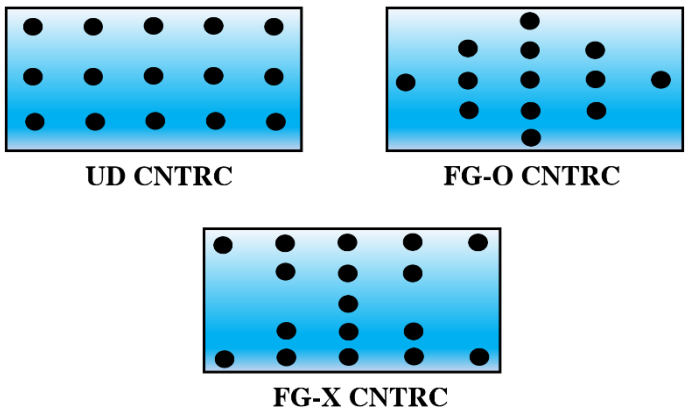

Figure 2. Cross-sections of various (CNTRC) carbon nanotube reinforced composite sandwich beams.

- FG-O CNTRC multilayered nanobeam:

$$V_{cnt} = 2\left(1 - \frac{\left|2|z| - \left|z_{(k-1)} + z_{(k)}\right|\right|}{z_{(k)} - z_{(k-1)}}\right) V^*_{cnt} \tag{2}$$

- FG-X CNTRC multilayered nanobeam:

$$V_{cnt} = 2\frac{\left|2|z| - \left|z_{(k-1)} + z_{(k)}\right|\right|}{z_{(k)} - z_{(k-1)}} V^*_{cnt} \tag{3}$$

More specifically, UD CNTRC refers to a uniform distribution of CNTs, whereas FG-V CNTRC, FG-O CNTRC and FG-X CNTRC account for different non-uniform FG distributions. Moreover, $z_{(k)}$ and $z_{(k\ -\ 1)}$ refer to the thickness coordinates at the bottom and top sides of the kth layer within the laminated nanobeam; V^*_{cnt} is the total volume fraction of CNTs, defined as

$$V^*_{cnt} = \frac{W_{cnt}}{W_{cnt} + (\rho_{cnt}/\rho_m)(1\ -\ W_{cnt})} \tag{4}$$

where W_{cnt} is the CNTs mass fraction; ρ_{cnt}, ρ_m refer to the CNTs and polymer mass density, respectively.

The Mori–Tanaka scheme [31] is here applied together with the rule of mixtures and molecular dynamics, as suggested in [1,2]. Thus, the effective Young's modulus and shear modulus for each CNTRC sheet is described as

$$\begin{array}{c} E_{11}^{k} = \eta_1 V_{cnt}^{k} E_{11}^{cnt} + V_{p}^{k} E_{p} \\ \frac{\eta_2}{E_{22}^{k}} = \frac{V_{cnt}^{k}}{E_{22}^{cnt}} + \frac{V_{p}^{k}}{E_{p}} \\ \frac{\eta_3}{G_{12}^{k}} = \frac{V_{cnt}^{k}}{G_{12}^{cnt}} + \frac{V_{p}^{k}}{G_{p}} \end{array} \tag{5}$$

where E_{11}^{k} and E_{22}^{k} are the elasticity modulus along the in-plane directions (x, z) for the kth layer and G_{12}^{k} is its shear modulus. The subscripts p and cnt refer to the polymer and SWCNT properties, respectively, assuming the CNT efficiency parameters η_1, η_2, η_3 as proposed in [6] and summarized in Table 1.

Table 1. CNT efficiency parameters.

V_{cnt}^{*}	η_1	η_2	η_3
0.12	0.137	1.022	0.715
0.17	0.142	1.626	1.138
0.28	0.141	1.585	1.109

The Poisson's ratio ν_{12}^{k}, the density ρ^{k}, and the thermal expansion coefficients in the longitudinal and transverse directions α_{11}^{k}, α_{22}^{k}, for each sheet are given as follows:

$$\nu_{12}^{k} = V_{cnt}^{k} \nu_{12}^{cnt} + V_{p}^{k} \nu_{p} \tag{6}$$

$$\rho^{k} = V_{cnt}^{k} \rho_{cnt} + V_{p}^{k} \rho_{p} \tag{7}$$

$$\alpha_{11}^{k} = V_{cnt}^{k} \alpha_{11}^{cnt} + V_{p}^{k} \alpha_{p} \tag{8}$$

$$\alpha_{22}^{k} = \left(1 + \nu_{12}^{cnt}\right) V_{cnt}^{k} \alpha_{22}^{cnt} + \left(1 + \nu_{p}\right) V_{p}^{k} \alpha_{p} \; - \; \nu_{12}^{k} \alpha_{11}^{k} \tag{9}$$

2.2. Kinematic Field

In the present work, a quasi-3D higher-order-shear deformation theory (HSDT) is used to define the governing equations for the buckling problem of CNTRC curved sandwich beams, whose displacements components are expressed in terms of the midline displacements and cross-section rotations as

$$\begin{array}{c} u(x,z,t) = \left(1 + \frac{z}{R}\right) u_0 \; - \; z \frac{\partial w_0}{\partial x} + \; \Phi(z) \varphi_x \\ w(x,z,t) = w_0 + \; \Phi(z)' \varphi_z \end{array} \tag{10}$$

A novel hyperbolic shape function $\Phi(z)$ is proposed herein to determine the distribution of the transverse shear strain and stress field along the thickness direction, namely

$$\Phi(z) = \frac{h\left(\pi \cos h\left(\frac{\pi}{2}\right) \tan h\left(\frac{z}{h}\right) \; - \; \sin h\left(\frac{\pi z}{h}\right)\left(1 \; - \; \tan h\left(\frac{1}{2}\right)^{2}\right)\right)}{\pi\left(\tan h\left(\frac{1}{2}\right)^{2} + \; \cos h\left(\frac{\pi}{2}\right) \; - \; 1\right)} \tag{11}$$

Based on a quasi-3D theory, the strain fields of the curved sandwich beam have the following form:

$$\begin{gathered}\varepsilon_{xx} = \left[\frac{\partial u}{\partial x} + \frac{w}{R}\right] = \frac{\partial u_0}{\partial x} - z\frac{\partial^2 w_0}{\partial x^2} + \Phi(z)\frac{\partial \varphi_x}{\partial x} + \frac{w_0}{R} + \Phi(z)'\frac{\varphi_z}{R} \\ \varepsilon_{zz} = \left[\frac{\partial w}{\partial x}\right] = \Phi(z)''\varphi_z \\ \gamma_{xz} = \left[\frac{\partial u}{\partial x} + \frac{\partial w}{\partial x} - \frac{u_0}{R}\right] = \Phi(z)'\left(\partial\varphi_x + \frac{\partial \varphi_z}{\partial x}\right)\end{gathered} \tag{12}$$

2.3. Constitutive Equations

The stress field is governed by the following constitutive relations:

$$\left\{\begin{array}{c}\sigma_{xx}\\ \sigma_{zz}\\ \tau_{xz}\end{array}\right\}^{(k)} = \left[\begin{array}{ccc}\overline{Q}^k_{11} & \overline{Q}^k_{13} & 0\\ \overline{Q}^k_{13} & \overline{Q}^k_{33} & 0\\ 0 & 0 & \overline{Q}^k_{55}\end{array}\right]\left\{\begin{array}{c}\varepsilon_{xx}\\ \varepsilon_{zz}\\ \gamma_{xz}\end{array}\right\}^{(k)} \tag{13}$$

with $\overline{Q}^k_{ij}$ being the transformed material constants, defined by means of the lamination angle θ_k for the kth layer, as follows:

$$\begin{gathered}\overline{Q}^k_{11} = Q_{11}\cos^4\theta_k + 2(Q_{12} + 2Q_{66})\sin^2\theta_k\cos^2\theta_k + Q_{22}\sin^4\theta_k \\ \overline{Q}^k_{13} = Q_{13}\cos^2\theta_k + Q_{23}\sin^2\theta_k \\ \overline{Q}^k_{55} = Q_{55}\cos^2\theta_k + Q_{44}\sin^2\theta_k\end{gathered} \tag{14}$$

and

$$\begin{gathered}Q_{11} = \frac{E_{11}}{1-\nu_{12}\nu_{21}} \\ Q_{12} = Q_{13} = \frac{\nu_{12}E_{11}}{1-\nu_{12}\nu_{21}} \\ Q_{23} = \frac{\nu_{21}E_{22}}{1-\nu_{12}\nu_{21}} \\ Q_{22} = Q_{33} = \frac{E_{22}}{1-\nu_{12}\nu_{21}}\end{gathered} \tag{15}$$

$$E_{33} = E_{22},\ G_{12} = G_{13} = G_{23},\ \nu_{21} = \frac{E_{22}}{E_{11}}\nu_{12},\ \nu_{13} = \nu_{12},\ \nu_{31} = \nu_{21},\ \nu_{32} = \nu_{23} = \nu_{21} \tag{16}$$

3. Equilibrium Governing Equations

3.1. Classical Formulation of Curved Sandwich Beams

Based on a classical formulation, the equilibrium equations of the problem are determined by means of the potential energy principle. In detail, the strain energy variation is defined as

$$\int_{-h/2}^{h/2}\int_0^L\left[\sigma^{(k)}_{xx}\delta\varepsilon_{xx} + \sigma^k_{zz}\varepsilon_{zz} + \tau^{(k)(k)}_{xz}\gamma_{xz}\right]\mathrm{d}x\mathrm{d}z - \int_0^L N^0_x\frac{\partial w_0}{\partial x}\frac{\partial\delta w_0}{\partial x}\mathrm{d}x - \int_0^L\left[k_w w_0\delta w_0 + k_g\frac{\partial w_0}{\partial x}\frac{\partial\delta w_0}{\partial x} + k_{NL}w_0^3\delta w_0\right]\mathrm{d}x \tag{17}$$

in agreement with a quasi-3D theory, where k_w and k_g are the linear Winkler stiffness and the shear layer stiffness, respectively, and k_{NL} refers to the non-linear stiffness. The strain energy variation can be rewritten in terms of stress resultants as

$$\int_0^L\left[N_{xx}\frac{\partial\delta u_0}{\partial x} - M_{xx}\frac{\partial^2\delta w_0}{\partial x^2} + P_{xx}\frac{\partial\delta\varphi_x}{\partial x} + N_{xx}\frac{\delta w_0}{R} + Q_x\frac{\delta\varphi_z}{R} + R_z\delta\varphi_z + Q_{xz}\delta\varphi_x + Q_{xz}\frac{\delta\delta\varphi_z}{\partial x}\right]\mathrm{d}x \tag{18}$$

where

$$
\begin{aligned}
N_{xx} &= \sum_{k=1}^{N} \int_{h_k}^{h_{k+1}} \sigma_{xx}^{(k)} \mathrm{d}z = A_{11} \frac{\partial u_0}{\partial x} - B_{11} \frac{\partial^2 w_0}{\partial x^2} + B_{11}^s \frac{\partial \varphi_x}{\partial x} + A_{11} \frac{w_0}{R} + D_{11} \frac{\varphi_z}{R} + E_{12} \varphi_z \\
M_{xx} &= \sum_{k=1}^{N} \int_{h_k}^{h_k+1} \sigma_{xx}^{(k)} z \mathrm{d}z = B_{11} \frac{\partial u_0}{\partial x} - F_{11} \frac{\partial^2 w_0}{\partial x^2} + F_{11}^s \frac{\partial \varphi_x}{\partial x} + B_{11} \frac{w_0}{R} + D_{11}^s \frac{\varphi_z}{R} + J_{12}^s \varphi_z \\
P_{xx} &= \sum_{k=1}^{N} \int_{h_k}^{h_k+1} \sigma_{xx}^{(k)} \Phi(z) \mathrm{d}z = B_{11}^s \frac{\partial u_0}{\partial x} - F_{11}^s \frac{\partial^2 w_0}{\partial x^2} + G_{11}^s \frac{\partial \varphi_x}{\partial x} + B_{11}^s \frac{w_0}{R} + H_{11}^s \frac{\varphi_z}{R} + E_{12}^s \varphi_z \\
Q_x &= \sum_{k=1}^{N} \int_{h_k}^{h_k+1} \sigma_{xx}^{(k)} \Phi(z)' \mathrm{d}z = D_{11} \frac{\partial u_0}{\partial x} - D_{11}^s \frac{\partial^2 w_0}{\partial x^2} + H_{11}^s \frac{\partial \varphi_x}{\partial x} + D_{11} \frac{w_0}{R} + K_{11}^s \frac{\varphi_z}{R} + L_{12}^s \varphi_z \\
Q_{xz} &= \sum_{k=1}^{N} \int_{h_k}^{h_k+1} \tau_{xz}^{(k)} \Phi(z)' \mathrm{d}z = K_{33}^s \left(\varphi_x + \frac{\partial \varphi_z}{\partial x} \right) \\
R_z &= \sum_{k=1}^{N} \int_{h_k}^{h_k+1} \sigma_{zz}^{(k)} \Phi(z)'' \mathrm{d}z = E_{12} \frac{\partial u_0}{\partial x} - E_{12}^s \frac{\partial^2 w_0}{\partial x^2} + J_{12}^s \frac{\partial \varphi_x}{\partial x} + E_{12} \frac{w_0}{R} + L_{12}^s \frac{\varphi_z}{R} + L_{22}^s \varphi_z
\end{aligned}
\tag{19}
$$

and

$$
\begin{aligned}
\left\{ A_{11},\ B_{11},\ F_{11},\ B_{11}^s, F_{11}^s, G_{11}^s \right\} &= \sum_{k=1}^{N} \int_{h_k}^{h_k+1} \overline{Q}_{11}^k \left\{ 1,\ z, z^2, \Phi(z), z\Phi(z), \Phi(z)^2 \right\} \mathrm{d}z \\
\left\{ D_{11}, D_{11}^s, H_{11}^s, K_{11}^s \right\} &= \sum_{k=1}^{N} \int_{h_k}^{h_k+1} \overline{Q}_{11}^k \left\{ \Phi(z)', z\Phi(z)', \Phi(z)\Phi(z)', \Phi(z)'^2 \right\} \mathrm{d}z \\
\left\{ E_{12},\ E_{12}^s,\ J_{12}^s,\ L_{12}^s \right\} &= \sum_{k=1}^{N} \int_{h_k}^{h_k+1} \overline{Q}_{12}^k \left\{ \Phi(z)'', z\Phi(z)'', \Phi(z)\Phi(z)'', \Phi(z)'\Phi(z)'' \right\} \mathrm{d}z \\
L_{22}^s &= \sum_{k=1}^{N} \int_{h_k}^{h_k+1} \overline{Q}_{22}^k \Phi(z)''^2 \mathrm{d}z \\
K_{33}^s &= \sum_{k=1}^{N} \int_{h_k}^{h_k+1} \overline{Q}_{33}^k \Phi(z)'^2 \mathrm{d}z
\end{aligned}
\tag{20}
$$

Integrating by parts and setting the coefficients of δu_0, δw_0, $\delta \varphi_x$, and $\delta \varphi_z$ equal to zero, the equilibrium equations of the problem are as follows:

$$
\begin{gathered}
\delta u_0 : \frac{\partial N_{xx}}{\partial x} = 0 \\
\delta w_0 : \frac{\partial^2 M_{xx}}{\partial x^2} - \frac{N_{xx}}{R} - N_x^0 \frac{\partial^2 w_0}{\partial x^2} - k_w w_0 + k_g \frac{\partial^2 w_0}{\partial x^2} - k_{NL} {w_0}^3 = 0 \\
\delta \varphi_x : \frac{\partial P_{xx}}{\partial x} - Q_{xz} = 0 \\
\delta \varphi_z : \frac{\partial Q_{xz}}{\partial x} - R_z - \frac{Q_x}{R} = 0
\end{gathered}
\tag{21}
$$

3.2. Nonlocal Strain Gradient Approach

We account for possible effects related to the strain gradient stress and nonlocal elastic stress fields, in line with [5], as follows:

$$
\sigma_{ij} = \sigma_{ij}^{(0)} - \frac{d\sigma_{ij}^{(1)}}{dx} \tag{22}
$$

where $\sigma_{ij}^{(0)}$ refers to the classical stress components corresponding to the strain field ε_{kl} and the higher-order stress $\sigma_{ij}^{(1)}$ corresponds to strain gradient $\varepsilon_{kl,x}$. The classical and higher-order stress components are described as

$$
\begin{aligned}
\sigma_{ij}^{(0)} &= \int_0^L C_{ijkl} \alpha_0(x, x', e_0 a) \varepsilon_{kl,x}(x') dx' \\
\sigma_{ij}^{(1)} &= l^2 \int_0^L C_{ijkl} \alpha_1(x, x', e_1 a) \varepsilon_{kl,x}(x') dx'
\end{aligned}
\tag{23}
$$

where C_{ijkl} is an elastic constant and l is the material length scale parameter, here introduced to account for the strain gradient stress field; e_0a and e_1a are the nonlocal parameters defining the nonlocal elastic stress field.

The nonlocal kernel functions $\alpha_0(x, x', e_0a)$ and $\alpha_1(x, x', e_1a)$ satisfy the conditions developed by Eringen [52], whereby the general constitutive relations can be defined as

$$\left[1 - (e_1a)^2\nabla^2\right]\left[1 - (e_0a)^2\nabla^2\right]\sigma_{ij} = C_{ijkl}\left[1 - (e_1a)^2\nabla^2\right]\varepsilon_{kl} - C_{ijkl}l^2\left[1 - (e_0a)^2\nabla^2\right]\nabla^2\varepsilon_{kl} \tag{24}$$

$$\left[1 - \mu\nabla^2\right]\sigma_{ij} = C_{ijkl}\left[1 - \lambda\nabla^2\right]\varepsilon_{kl} \tag{25}$$

where $\mu = (ea)^2$ and $\lambda = l^2$.

In addition, the constitutive relations for a nonlocal shear deformable CNTRC curved sandwich nanobeam can be written as

$$\sigma_{xx} - \mu\frac{\partial^2\sigma_{xx}}{\partial x^2} = \overline{Q}_{11}^k\left(\varepsilon_{xx} - \lambda\frac{\partial^2\varepsilon_{xx}}{\partial x^2}\right) \tag{26}$$

$$\sigma_{xz} - \mu\frac{\partial^2\sigma_{xx}}{\partial x^2} = \overline{Q}_{55}^k\left(\gamma_{xz} - \lambda\frac{\partial^2\gamma_{xz}}{\partial x^2}\right) \tag{27}$$

Based on a nonlocal strain gradient theory, the following equilibrium equations are obtained in terms of the displacement components by substitution of Equation (19) into Equation (21).

$$\begin{gathered}
\left(1 - \lambda\tfrac{\partial^2}{\partial x^2}\right)\left(A_{11}\tfrac{\partial^2 u_0}{\partial x^2} - B_{11}\tfrac{\partial^3 w_0}{\partial x^3} + \tfrac{A_{11}}{R}\tfrac{\partial w_0}{\partial x} + B_{11}^s\tfrac{\partial^2\varphi_x}{\partial x^2} + \left(\tfrac{D_{11}}{R} + E_{12}\right)\tfrac{\partial\varphi_z}{\partial x}\right) = 0 \\
\left(1 - \lambda\tfrac{\partial^2}{\partial x^2}\right)\left(\begin{array}{c} B_{11}\tfrac{\partial^3 u_0}{\partial x^3} - \tfrac{A_{11}}{R}\tfrac{\partial u_0}{\partial x} - F_{11}\tfrac{\partial^4 w_0}{\partial x^4} + \tfrac{2B_{11}}{R}\tfrac{\partial^2 w_0}{\partial x^2} - \tfrac{A_{11}}{R^2}w_0 \\ + F_{11}^s\tfrac{\partial^3\varphi_x}{\partial x^3} - \tfrac{B_{11}^s}{R}\tfrac{\partial\varphi_x}{\partial x} + \left(\tfrac{D_{11}^s}{R} + J_{12}^s\right)\tfrac{\partial^2\varphi_z}{\partial x^2} - \left(\tfrac{D_{11}}{R^2} + \tfrac{E_{12}}{R}\right)\varphi_z \end{array}\right) \\
- \left(1 - \mu\tfrac{\partial^2}{\partial x^2}\right)\left(N_x^0\tfrac{\partial^2 w_0}{\partial x^2} - k_w w_0 - k_g\tfrac{\partial^2 w_0}{\partial x^2} - k_w {w_0}^3\right) = 0 \\
\left(1 - \lambda\tfrac{\partial^2}{\partial x^2}\right)\left(B_{11}^s\tfrac{\partial^2 u_0}{\partial x^2} - F_{11}^s\tfrac{\partial^3 w_0}{\partial x^3} + \tfrac{B_{11}^s}{R}\tfrac{\partial w_0}{\partial x} + G_{11}^s\tfrac{\partial^2\varphi_x}{\partial x^2} - K_{33}^s\varphi_x + \left(\tfrac{H_{11}^s}{R} + J_{12}^s - K_{33}^s\right)\tfrac{\partial\varphi_z}{\partial x}\right) = 0 \\
\left(1 - \lambda\tfrac{\partial^2}{\partial x^2}\right)\left(\begin{array}{c} -\left(\tfrac{D_{11}}{R} - E_{12}\right)\tfrac{\partial u_0}{\partial x} + \left(\tfrac{D_{11}^s}{R} + E_{12}^s\right)\tfrac{\partial^2 w_0}{\partial x^2} - \left(\tfrac{D_{11}}{R^2} + \tfrac{E_{12}}{R}\right)w_0 \\ -\left(\tfrac{H_{11}^s}{R} + J_{12}^s - K_{33}^s\right)\tfrac{\partial\varphi_x}{\partial x} - \left(2\tfrac{L_{12}^s}{R} + \tfrac{K_{11}^s}{R^2} + L_{22}^s\right)\varphi_z + K_{33}^s\tfrac{\partial^2\varphi_z}{\partial x^2} \end{array}\right) = 0
\end{gathered} \tag{28}$$

3.3. Temperature Field

In the present work we assume a uniform temperature field distribution on the CNTRC surfaces, labeled as T_m and T_p, on the bottom and top sandwich surfaces, respectively. A (10,10) SWCNT-based reinforcement is selected within the numerical investigation, with the same mechanical properties as assumed by Shen [4] and summarized in Table 2.

Table 2. Thermo-mechanical properties of SWCNTs.

T[K]	E_{11}^{cnt}[TPa]	E_{22}^{cnt}[TPa]	G_{12}^{cnt}[TPa]	ν_{11}^{cnt}	$\alpha_{11}^{cnt}[10^{-6}]$/K]	$\alpha_{22}^{cnt}[10^{-6}]$/K]
300	5.6466	7.0800	1.9445	0.175	3.4584	5.1682
400	5.5679	6.9814	1.9703	0.175	4.1496	5.0905
500	5.5308	6.9348	1.9643	0.175	4.5361	5.0189
700	5.4744	6.8641	1.9644	0.175	4.6677	4.8943
1000	5.2814	6.6220	1.9451	0.175	4.2800	4.7532

To analyze the thermal effect on the buckling response of CNTRC curved sandwich nanobeams, we assume the following temperature-dependent material properties, in line with [53].

$$P = P_0\left(P_{-1}T^{-1} + 1 + P_1T + P_2T^2 + P_3T^3 + P_4T^4\right) \quad (29)$$

where $T = T_0 + \Delta T$, T_0 is the ambient temperature ($T_0 = 300$ K), ΔT is the temperature difference, and P_0, P_1, P_2, P_3 and P_4 are thermal coefficients listed in Table 3.

Table 3. Temperature-dependent coefficients of CNT material properties [22].

	P_0	P_{-1}	P_1	P_2	P_3	P_4
E_{11}^{cnt} [TPa]	6.5653	0	-8.9437×10^{-4}	1.9182×10^{-6}	-1.8198×10^{-9}	6.0043×10^{-13}
E_{22}^{cnt} [TPa]	8.2271	0	-8.9024×10^{-4}	1.9066×10^{-6}	-1.8063×10^{-9}	5.9486×10^{-13}
G_{12}^{cnt} [TPa]	1.1056	0	5.6727×10^{-3}	-1.4815×10^{-5}	1.6402×10^{-8}	-6.5007×10^{-12}
$\alpha_{11}\left[10^{-6}/^{\circ}C\right]$	−1.1279	0	-2.0340×10^{-2}	2.5672×10^{-5}	-1.0186×10^{-8}	5.9455×10^{-14}
$\alpha_{22}\left[10^{-6}/^{\circ}C\right]$	5.4359	0	-1.7906×10^{-4}	4.6367×10^{-8}	1.2424×10^{-11}	-5.3290×10^{-14}
ν_{12}^{cnt}	0.175	0	0	0	0	0

The polymeric matrix (PmPV) features temperature-dependent elastic properties, as follows:

$$E_m = (3.51 - 0.0047T)\ \text{GPa} \quad (30)$$

$$\alpha_m = 45(1 + 0.0005\Delta T)10^{-6}\ \text{GPa} \quad (31)$$

where the Poisson's ratio and mass density are set as $v_m = 0.34$ and $\rho_m = 1150\ \text{kg/m}^3$, respectively.

4. Analytical Solution

In this section, the equilibrium equations are solved analytically using the Galerkin method for simply-supported (SS), clamped-clamped (CC) and clamped-hinged (CS) boundary conditions. The following displacement functions are thus assumed:

$$\begin{Bmatrix} u_0 \\ w_0 \\ \varphi_x \\ \varphi_z \end{Bmatrix} = \sum_{m=1}^{\infty} \begin{Bmatrix} U_m \frac{\partial X_m}{\partial x} \\ W_m X_m \\ \psi_{xm} \frac{\partial X_m}{\partial x} \\ \psi_{zm} X_m \end{Bmatrix} \quad (32)$$

with U_m, W_m, ψ_{xm} and ψ_{zm} being arbitrary parameters. The functions $X_m(x)$ that satisfy the selected boundary conditions are defined as

- For SS beam

$$X_m = \sin(\beta x),\ \ \beta = \frac{m\pi}{L} \quad (33)$$

- For CC beam

$$X_m = 1 - \cos(\beta x)\ \ , \beta = \frac{2m\pi}{L} \quad (34)$$

- For CS beam

$$X_m = \sin(\beta x)[\cos(\beta x) - 1],\ \ \beta = \frac{m\pi}{L} \quad (35)$$

By substituting Equation (32) in Equation (28), we get

$$[K_{ij}]\begin{Bmatrix} U_m \\ W_m \\ \psi_{xm} \\ \psi_{zm} \end{Bmatrix} = 0, \quad i,j = 1:4 \tag{36}$$

where

$$K_{11} = A_{11}\left(\int_0^L \frac{\partial^3 X_m}{\partial x^3}\frac{\partial X_m}{\partial x}\mathrm{d}x - \lambda\int_0^L \frac{\partial^5 X_m}{\partial x^5}\frac{\partial X_m}{\partial x}\mathrm{d}x\right)$$

$$K_{12} = -B_{11}\left(\int_0^L \frac{\partial^3 X_m}{\partial x^3}\frac{\partial X_m}{\partial x}\mathrm{d}x - \lambda\int_0^L \frac{\partial^5 X_m}{\partial x^5}\frac{\partial X_m}{\partial x}\mathrm{d}x\right) + \frac{A_{11}}{R}\left(\int_0^L \left(\frac{\partial X_m}{\partial x}\right)^2\mathrm{d}x - \lambda\int_0^L \frac{\partial^3 X_m}{\partial x^3}\frac{\partial X_m}{\partial x}\mathrm{d}x\right)$$

$$K_{13} = B_{11}^S\left(\int_0^L \frac{\partial^3 X_m}{\partial x^3}\frac{\partial X_m}{\partial x}\mathrm{d}x - \lambda\int_0^L \frac{\partial^5 X_m}{\partial x^5}\frac{\partial X_m}{\partial x}\mathrm{d}x\right)$$

$$K_{14} = \left(\frac{D_{11}}{R} + E_{12}\right)\left(\int_0^L \left(\frac{\partial X_m}{\partial x}\right)^2\mathrm{d}x - \lambda\int_0^L \frac{\partial^3 X_m}{\partial x^3}\frac{\partial X_m}{\partial x}\mathrm{d}x\right)$$

$$K_{21} = B_{11}\left(\int_0^L \frac{\partial^4 X_m}{\partial x^4}X_m\mathrm{d}x - \lambda\int_0^L \frac{\partial^6 X_m}{\partial x^6}X_m\mathrm{d}x\right) - \frac{A_{11}}{R}\left(\int_0^L \frac{\partial^2 X_m}{\partial x^2}X_m\mathrm{d}x - \lambda\int_0^L \frac{\partial^4 X_m}{\partial x^4}X_m\mathrm{d}x\right)$$

$$K_{22} = -F_{11}\left(\int_0^L \frac{\partial^4 X_m}{\partial x^4}X_m\mathrm{d}x - \lambda\int_0^L \frac{\partial^6 X_m}{\partial x^6}X_m\,\mathrm{d}x\right) + 2\frac{B_{11}}{R}\left(\int_0^L \frac{\partial^2 X_m}{\partial x^2}X_m\mathrm{d}x - \lambda\int_0^L \frac{\partial^4 X_m}{\partial x^4}X_m\,\mathrm{d}x\right) - \left(N_x^0 - k_g\right)\left(\int_0^L \frac{\partial^2 X_m}{\partial x^2}X_m\mathrm{d}x - \right. \tag{37}$$

$$\left.\mu\int_0^L \frac{\partial^4 X_m}{\partial x^4}X_m\,\mathrm{d}x\right) - k_w\left(\int_0^L {X_m}^2\mathrm{d}x - \mu\int_0^L \frac{\partial^2 X_m}{\partial x^2}X_m\mathrm{d}x\right) - k_{NL}\left(\int_0^L {X_m}^4\mathrm{d}x - \mu\int_0^L \frac{\partial^2 {X_m}^3}{\partial x^2}X_m\mathrm{d}x\right)$$

$$K_{23} = F_{11}^S\left(\int_0^L \frac{\partial^4 X_m}{\partial x^4}X_m\mathrm{d}x - \lambda\int_0^L \frac{\partial^6 X_m}{\partial x^6}X_m\,\mathrm{d}x\right) - \frac{B_{11}^S}{R}\left(\int_0^L \frac{\partial^2 X_m}{\partial x^2}X_m\mathrm{d}x - \lambda\int_0^L \frac{\partial^4 X_m}{\partial x^4}X_m\,\mathrm{d}x\right)$$

$$K_{24} = \left(\frac{D_{11}^S}{R} + E_{12}^S\right)\left(\int_0^L \frac{\partial^2 X_m}{\partial x^2}X_m\mathrm{d}x - \lambda\int_0^L \frac{\partial^4 X_m}{\partial x^4}X_m\mathrm{d}x\right) - \left(\frac{D_{11}}{R^2} + \frac{E_{12}}{R}\right)\left(\int_0^L {X_m}^2\mathrm{d}x - \lambda\int_0^L \frac{\partial^2 X_m}{\partial x^2}X_m\mathrm{d}x\right)$$

$$K_{31} = B_{11}^S\left(\int_0^L \frac{\partial^3 X_m}{\partial x^3}\frac{\partial X_m}{\partial x}\mathrm{d}x - \lambda\int_0^L \frac{\partial^5 X_m}{\partial x^5}\frac{\partial X_m}{\partial x}\mathrm{d}x\right)$$

$$K_{32} = -F_{11}^S\left(\int_0^L \frac{\partial^3 X_m}{\partial x^3}\frac{\partial X_m}{\partial x}\mathrm{d}x - \lambda\int_0^L \frac{\partial^5 X_m}{\partial x^5}\frac{\partial X_m}{\partial x}\mathrm{d}x\right) - \frac{B_{11}^S}{R}\left(\int_0^L \frac{\partial {X_m}^2}{\partial x}\mathrm{d}x - \lambda\int_0^L \frac{\partial^3 X_m}{\partial x^3}\frac{\partial X_m}{\partial x}\mathrm{d}x\right)$$

$$K_{33} = G_{11}^S\left(\int_0^L \frac{\partial^3 X_m}{\partial x^3}\frac{\partial X_m}{\partial x}\mathrm{d}x - \lambda\int_0^L \frac{\partial^5 X_m}{\partial x^5}\frac{\partial X_m}{\partial x}\mathrm{d}x\right) - K_{33}^S\left(\int_0^L \left(\frac{\partial X_m}{\partial x}\right)^2\mathrm{d}x - \lambda\int_0^L \frac{\partial^3 X_m}{\partial x^3}\frac{\partial X_m}{\partial x}\mathrm{d}x\right)$$

$$K_{34} = \left(\frac{H_{11}^S}{R} + J_{12}^S - K_{33}^S\right)\left(\int_0^L \left(\frac{\partial X_m}{\partial x}\right)^2\mathrm{d}x - \lambda\int_0^L \frac{\partial^3 X_m}{\partial x^3}\frac{\partial X_m}{\partial x}\mathrm{d}x\right)$$

$$K_{41} = -\left(\frac{D_{11}}{R} + E_{12}\right)\left(\int_0^L \frac{\partial^2 X_m}{\partial x^2}X_m\mathrm{d}x - \lambda\int_0^L \frac{\partial^4 X_m}{\partial x^4}X_m\,\mathrm{d}x\right)$$

$$K_{42} = \left(\frac{D_{11}^S}{R} + E_{12}^S\right)\left(\int_0^L \frac{\partial^2 X_m}{\partial x^2}X_m\mathrm{d}x - \lambda\int_0^L \frac{\partial^4 X_m}{\partial x^4}X_m\,\mathrm{d}x\right) - \left(\frac{D_{11}}{R^2} + \frac{E_{12}}{R}\right)\left(\int_0^L {X_m}^2\mathrm{d}x - \lambda\int_0^L \frac{\partial^2 X_m}{\partial x^4}X_m\,\mathrm{d}x\right)$$

$$K_{43} = -\left(\frac{H_{11}^S}{R} + J_{12}^S - K_{33}^S\right)\left(\int_0^L \frac{\partial^2 X_m}{\partial x^2}X_m\mathrm{d}x - \lambda\int_0^L \frac{\partial^4 X_m}{\partial x^4}X_m\,\mathrm{d}x\right)$$

$$K_{44} = -\left(2\frac{L_{12}^S}{R} + \frac{K_{11}^S}{R^2} + L_{22}^S\right)\left(\int_0^L {X_m}^2\mathrm{d}x - \lambda\int_0^L \frac{\partial^2 X_m}{\partial x^2}X_m\,\mathrm{d}x\right) + K_{33}^S\left(\int_0^L \frac{\partial^2 X_m}{\partial x^2}X_m\mathrm{d}x - \lambda\int_0^L \frac{\partial^4 X_m}{\partial x^4}X_m\,\mathrm{d}x\right)$$

The accuracy of the proposed theoretical solution is explored in the next section, within a large systematic investigation aimed at determining the sensitivity of the buckling response. The proposed model is limited to uniform cross-sectional curved FG-CNTRC nanobeams with SS, SC, and CC boundary conditions and linear variation of temperature across the beam thickness; a further expansion should include more complicated cross-sectional geometries and thermal variations.

5. Results and Discussion

In this section, various numerical applications are presented to determine the accuracy of a quasi-3D HSDT, to solve the buckling problem of FG-CNTRC straight sandwich beams, compared to some existing solutions from the literature. Then, we investigate the effect of curvature on the structural response of CNTRC sandwich beams, which could be of great interest for design purposes, among different engineering applications. In what follows, the critical buckling load and elastic foundation parameters are presented in dimensionless form, as follows:

$$\overline{N} = R^2 \frac{N_x^0}{A_{110}}, \qquad K_w = \frac{k_w L^2}{A_{110}}, \qquad K_g = \frac{k_g}{A_{110}}, \qquad K_{NL} = \frac{k_{NL} L^2}{A_{110}} \tag{38}$$

where the coefficient A_{110} refers to a beam made of pure matrix material at room temperature T = 300 K. The length of the curved sandwich beam is kept equal to L = 20 for all the numerical examples.

5.1. Comparison Study

We start the numerical analysis by a comparative evaluation of our results with predictions from the open literature, while including possible thickness stretching effects. In Table 4, we summarize the results in terms of dimensionless critical buckling load for SS- and CC-CNTRC sandwich beams with and without thickness stretching effects and compare their accuracy against the numerical predictions by Wu et al. [6], based on a differential quadrature method (DQM). The face sheets are made of poly methyl methacrylate (PMMA) as matrix, with $E_m = 2.5$ GPa and $\nu_m = 0.3$, and armchair (10, 10) SWCNTs as reinforcement phase, with $E_{11}^{cnt} = 5.6466$ TPa, $E_{22}^{cnt} = 7.08$ TPa, $G_{12}^{cnt} = 1.9445$ TPa and $\nu_{cnt} = 0.175$ (in 300 K). Titanium alloy (Ti-6Al-4V) is used as core, with $E_m = 113.8$ GPa and $\nu_m = 0.342$. It is worth noticing the good correlation between our results (see Table 4) and the findings of [6] when the thickness stretching effect is neglected.

5.2. Parametric Study

The parametric study in this section assumes a PmPV as core material and as matrix phase for the face sheets of the sandwich structure, with mechanical properties as specified in Equations (30) and (31); (10,10) SWCNTs are considered as the reinforcement phase (Table 3). The mechanical properties of materials depend on the temperature. Table 5 presents the effect of the dimensionless thickness ratio L/h on the buckling load of a single layer CNTRC curved beam with various CNT volume fractions in the presence (or absence) of a thickness stretching effect ε_{zz}, while keeping the opening angle $\alpha = L/R$ equal to $\pi/3$. Note that increased values of L/h result in lower values of the buckling load, under the same assumptions for the reinforcement distribution, volume fraction and possible stretching effects. In any case, the worst buckling response is observed for an FG-O reinforcement distribution within the material, whereas a FG-X distribution seems to yield the highest buckling loads for fixed values of L/h, ε_{zz}, V_{cnt}^*. The stability of the curved beam increases significantly for higher values of V_{cnt}^*, with a small variation in the buckling load, depending on whether ε_{zz} is assumed (or not) equal to zero.

Table 4. Comparisons of dimensionless critical buckling loads for FG-CNTRC straight beams h_c/h_f, $V^*_{cnt} = 0.12$.

	L/h		CC			SS		
			V^*_{cnt}=12	V^*_{cnt}=17	V^*_{cnt}=28	V^*_{cnt}=12	V^*_{cnt}=17	V^*_{cnt}=28
UD	10	Wu [6]	0.0254	0.0296	0.0373	0.0070	0.0082	0.0107
		Present $\varepsilon_{zz} = 0$	0.0271	0.0319	0.0413	0.0071	0.0084	0.0110
		Present $\varepsilon_{zz} \neq 0$	0.0267	0.0316	0.0410	0.0066	0.0080	0.0106
	20	Wu [6]	0.0070	0.0082	0.0107	0.0018	0.0021	0.0028
		Present $\varepsilon_{zz} = 0$	0.0071	0.0084	0.0110	0.0018	0.0021	0.0028
		Present $\varepsilon_{zz} \neq 0$	0.0069	0.0082	0.0108	0.0017	0.0020	0.0027
	30	Wu [6]	0.0031	0.0037	0.0049	0.0008	0.0009	0.0012
		Present $\varepsilon_{zz} = 0$	0.0032	0.0038	0.0049	0.0008	0.0009	0.0012
		Present $\varepsilon_{zz} \neq 0$	0.0031	0.0037	0.0049	0.0007	0.0008	0.0012
FG	10	Wu [6]	0.0261	0.0305	0.0387	0.0072	0.0085	0.0111
		Present $\varepsilon_{zz} = 0$	0.0271	0.0319	0.0413	0.0071	0.0084	0.0110
		Present $\varepsilon_{zz} \neq 0$	0.0267	0.0316	0.0410	0.0066	0.0079	0.0106
	20	Wu [6]	0.0072	0.0085	0.0111	0.0018	0.0022	0.0029
		Present $\varepsilon_{zz} = 0$	0.0071	0.0084	0.0110	0.0018	0.0021	0.0028
		Present $\varepsilon_{zz} \neq 0$	0.0069	0.0082	0.0108	0.0017	0.0020	0.0027
	30	Wu [6]	0.0032	0.0039	0.0051	0.0008	0.0010	0.0013
		Present $\varepsilon_{zz} = 0$	0.0032	0.0038	0.0049	0.0008	0.0010	0.0012
		Present $\varepsilon_{zz} \neq 0$	0.0031	0.0037	0.0049	0.0007	0.0009	0.0012

Table 5. Effect of thickness ratio on the buckling load of a single layer CNTRC curved beam $\alpha = \frac{\pi}{3}$, T = 300 K.

	L/h	V^*_{cnt}=12		V^*_{cnt}=17		V^*_{cnt}=28	
		ε_{zz}=0	$\varepsilon_{zz}\neq$0	ε_{zz}=0	$\varepsilon_{zz}\neq$0	ε_{zz}=0	$\varepsilon_{zz}\neq$0
UD	5	73.7930	73.4424	120.6917	120.1610	146.3642	145.5590
	10	49.0266	49.0250	77.6401	77.6399	101.4712	101.4484
	20	21.9451	21.9242	33.2103	33.1708	48.7346	48.7136
	30	11.4565	11.4369	17.0329	16.9992	26.2191	26.1931
FG-X	5	79.5433	79.1094	128.5687	127.9463	149.0114	148.3479
	10	57.1285	57.1134	90.5184	90.5055	111.0156	110.9778
	20	28.9721	28.9611	44.1395	44.1160	61.6479	61.6372
	30	15.9804	15.9653	23.8972	23.8700	35.6810	35.6608
FG-O	5	58.0980	57.9593	96.1446	95.9410	128.1600	127.5412
	10	33.6793	33.6650	52.7577	52.7221	75.9965	75.9952
	20	12.7261	12.6870	18.9830	18.9144	29.3401	29.2905
	30	6.2518	6.2261	9.1882	9.1452	14.5124	14.4755

In Table 6, we account for the influence of opening angles α, boundary conditions, and CNT reinforcement patterns on the dimensionless critical buckling load of $(0^\circ/90^\circ/c/90^\circ/0^\circ)$

sandwich beams. Note that the critical buckling load increases significantly for a decreased opening angle and increased CNT volume fraction. As summarized in Table 7, the dimensionless critical buckling load of curved sandwich $(0°/90°/0°/c/0°/90°/0°)$ nanobeams could be affected by nonlocal and length scale parameters as well as by the core-to-face sheet thickness ratio, h_c/h_f, and thermal condition. A meaningful reduction of the critical buckling load is observed for higher temperatures for a fixed geometry and nonlocal parameters μ, λ. An increased value of μ and a reduced value of λ reduce the critical buckling load of the nanostructure under the same thermal and geometric assumptions. Moreover, Table 8 summarizes the sensitivity of the buckling response of CNTRC sandwich $(0°/c/0°)$ beams to different elastic foundation parameters and boundary conditions, with an increased stability of the structure for more rigid boundary conditions and foundation.

Table 6. Effect of opening angle on the dimensionless buckling load of curved sandwich beam $(0°/90°/c/90°/0°)$ ($h_c/h_f = 4$, $h = L/10$, $T = 300$ K.

	α	SS			CC			CS		
		V^*_{cnt}=12	V^*_{cnt}=17	V^*_{cnt}=28	V^*_{cnt}=12	V^*_{cnt}=17	V^*_{cnt}=28	V^*_{cnt}=12	V^*_{cnt}=17	V^*_{cnt}=28
UD	$\pi/4$	74.6585	100.3288	139.9486	339.9366	442.8754	611.3111	212.5558	278.2913	381.2890
	$\pi/3$	41.9954	56.4350	78.7211	257.7059	343.7374	492.5488	149.4863	199.1205	281.3863
	$\pi/2$	18.6646	25.0822	34.9871	198.9635	272.9172	407.7090	104.4352	142.5681	210.0248
	$2\pi/3$	10.4989	14.1087	19.6803	178.3950	248.1198	378.0018	88.6652	122.7722	185.0451
FG-X	$\pi/4$	74.8276	100.6190	140.6169	340.6800	444.0969	613.9162	213.0218	279.0764	383.0227
	$\pi/3$	42.0905	56.5982	79.0970	258.1393	344.4732	494.1862	149.7553	199.5840	282.4389
	$\pi/2$	18.7069	25.1548	35.1542	199.1755	273.3061	408.6553	104.5634	142.8020	210.5910
	$2\pi/3$	10.5226	14.1496	19.7743	178.5296	248.3875	378.7063	88.7442	122.9258	185.4411
FG-O	$\pi/4$	74.5146	100.1307	139.7518	339.3283	442.1373	610.8484	212.1712	277.8003	380.9295
	$\pi/3$	41.9144	56.3235	78.6104	257.3788	343.3707	492.4602	149.2768	198.8661	281.2614
	$\pi/2$	18.6286	25.0327	34.9379	198.8371	272.8157	407.8875	104.3507	142.4828	210.0675
	$2\pi/3$	10.4786	14.0809	19.6526	178.3388	248.1110	378.2735	88.6244	122.7461	185.1463

Table 7. Effect of nonlocal and length scale parameter on the dimensionless buckling load of simply supported UD-CNTRC curved sandwich nanobeam $(0°/90°/0°/c/0°/90°/0°)$ ($\alpha = \pi/3$, $h = L/10$, $V^*_{cnt} = 28$.

μ		h_c/h_f								
		T = 300 K			T = 500 K			T = 700 K		
	λ	4	6	8	4	6	8	4	6	8
0	0	81.8686	73.5399	66.3319	61.1267	56.6032	52.3027	19.0516	18.8260	18.5363
	1	83.8886	75.3545	67.9686	62.6350	57.9999	53.5932	19.5217	19.2906	18.9937
	2	85.9086	77.1690	69.6053	64.1432	59.3965	54.8837	19.9918	19.7551	19.4511
	3	87.9287	78.9835	71.2419	65.6515	60.7931	56.1743	20.4618	20.2196	19.9084
1	0	79.8972	71.7691	64.7347	59.6548	55.2402	51.0433	18.5928	18.3727	18.0900
	1	81.8686	73.5399	66.3319	61.1267	56.6032	52.3027	19.0516	18.8260	18.5363
	2	83.8400	75.3108	67.9292	62.5987	57.9662	53.5622	19.5104	19.2794	18.9827
	3	85.8114	77.0816	69.5265	64.0706	59.3292	54.8216	19.9691	19.7327	19.4290
2	0	78.0185	70.0816	63.2125	58.2521	53.9413	49.8431	18.1557	17.9407	17.6646
	1	79.9436	71.8107	64.7722	59.6894	55.2723	51.0729	18.6036	18.3834	18.1005
	2	81.8686	73.5399	66.3319	61.1267	56.6032	52.3027	19.0516	18.8260	18.5363
	3	83.7936	75.2691	67.8916	62.5640	57.9342	53.5325	19.4996	19.2687	18.9722
3	0	76.2262	68.4715	61.7603	56.9139	52.7021	48.6980	17.7386	17.5285	17.2588
	1	78.1070	70.1610	63.2842	58.3181	54.0025	49.8996	18.1762	17.9610	17.6847
	2	79.9878	71.8505	64.8081	59.7224	55.3029	51.1011	18.6139	18.3935	18.1105
	3	81.8686	73.5399	66.3319	61.1267	56.6032	52.3027	19.0516	18.8260	18.5363

Table 8. Effect of hardening nonlinear parameters on the dimensionless buckling load of CNTRC curved sandwich beams $(0^\circ/c/0^\circ)$ ($\alpha = \pi/3$, $h = L/10$, $h_c/h_f = 4$, $V^*_{cnt} = 0.12$, $T = 300$ K.

K_w	K_g	K_{nl}	SS			CC			CS		
			UD	FG-X	FG-O	UD	FG-X	FG-O	UD	FG-X	FG-O
0	0	0	59.3208	59.9622	58.6879	406.4881	408.7038	404.3375	229.0790	230.5969	227.5994
		0.05	60.7067	61.3482	60.0738	410.5303	412.7460	408.3797	230.5082	232.0261	229.0286
		0.1	62.0926	62.7341	61.4597	414.5725	416.7882	412.4220	231.9374	233.4554	230.4578
	0.05	0	77.5586	78.2001	76.9257	424.7259	426.9416	422.5753	247.3168	248.8347	245.8372
		0.05	78.9446	79.5860	78.3117	428.7681	430.9838	426.6175	248.7460	250.2640	247.2664
		0.1	80.3305	80.9719	79.6976	432.8103	435.0261	430.6598	250.1752	251.6932	248.6957
	0.1	0	95.7965	96.4379	95.1636	442.9637	445.1794	440.8131	265.5546	267.0725	264.0750
		0.05	97.1824	97.8238	96.5495	447.0059	449.2216	444.8554	266.9838	268.5018	265.5042
		0.1	98.5683	99.2097	97.9354	451.0482	453.2639	448.8976	268.4130	269.9310	266.9335
0.05	0	0	61.1687	61.8101	60.5358	407.8740	410.0897	405.7234	230.2339	231.7518	228.7543
		0.05	62.5546	63.1960	61.9217	411.9162	414.1319	409.7656	231.6631	233.1811	230.1835
		0.1	63.9405	64.5819	63.3076	415.9584	418.1742	413.8079	233.0923	234.6103	231.6128
	0.05	0	79.4065	80.0479	78.7736	426.1118	428.3275	423.9612	248.4717	249.9897	246.9921
		0.05	80.7924	81.4338	80.1595	430.1540	432.3697	428.0034	249.9009	251.4189	248.4214
		0.1	82.1783	82.8197	81.5454	434.1962	436.4120	432.0457	251.3301	252.8481	249.8506
	0.1	0	97.6443	98.2857	97.0114	444.3496	446.5653	442.1990	266.7095	268.2275	265.2300
		0.05	99.0302	99.6717	98.3973	448.3918	450.6076	446.2413	268.1387	269.6567	266.6592
		0.1	100.4162	101.0576	99.7833	452.4341	454.6498	450.2835	269.5680	271.0859	268.0884
0.1	0	0	63.0166	63.6580	62.3837	409.2599	411.4756	407.1093	231.3888	232.9068	229.9092
		0.05	64.4025	65.0439	63.7696	413.3021	415.5178	411.1515	232.8180	234.3360	231.3385
		0.1	65.7884	66.4298	65.1555	417.3443	419.5601	415.1938	234.2473	235.7652	232.7677
	0.05	0	81.2544	81.8958	80.6215	427.4977	429.7134	425.3471	249.6266	251.1446	248.1471
		0.05	82.6403	83.2817	82.0074	431.5399	433.7556	429.3894	251.0559	252.5738	249.5763
		0.1	84.0262	84.6676	83.3933	435.5822	437.7979	433.4316	252.4851	254.0030	251.0055
	0.1	0	99.4922	100.1336	98.8593	445.7355	447.9512	443.5849	267.8645	269.3824	266.3849
		0.05	100.8781	101.5195	100.2452	449.7777	451.9935	447.6272	269.2937	270.8116	267.8141
		0.1	102.2640	102.9054	101.6311	453.8200	456.0357	451.6694	270.7229	272.2408	269.2433

Figure 3 also depicts the buckling response for a SS $(0^\circ/90^\circ/c/90^\circ/0^\circ)$ beam versus the thickness ratio, L/h, while varying the opening angles. All the plots in Figure 3 feature a monotone decreasing behavior for increasing values of L/h, reaching a plateau for $L/h \geq 30$. Note also that an increased opening angle value decreases significantly the buckling load of the structure for each fixed value of L/h.

In Figure 4 the critical buckling load versus the opening angle is illustrated, taking into account the core-to-face sheet thickness ratio variation. A clear reduction of the beam stiffness with an increased core layer can be observed for each fixed opening angle, which is even more pronounced for lower values of the opening angles.

Figure 5 also shows the double effect of the core-to-face sheet thickness ratio and CNT volume fraction on the dimensionless buckling load, with a clear shift of the curve upwards for increasing values of V_{cnt}. The highest critical buckling load is reached for a volume fraction $V_{cnt} = 28$, where the lowest stability is observed for $V_{cnt} = 12$. The impact of the thermal environment on critical buckling load is visible in Figure 6, where an increased temperature value leads to a clear reduction in the buckling load for all the selected boundary conditions because of the thermal dependence of the mechanical properties of the materials. As also expected, the highest stability is reached by CC sandwich beams, independently of the thermal environment. The further effect of nonlocal μ and length scale λ parameters on the critical buckling load is also plotted in Figures 7 and 8, respectively. One can easily note that the buckling load increases by decreasing the nonlocal parameter and by increasing the length scale parameter, in line with the information in Table 7. Unlike the length scale

parameter λ, an increased nonlocal parameter μ leads to a stiffness reduction of CNTRC laminated nanobeams. The critical buckling load versus the thickness ratio L/h is finally illustrated in Figure 9 by assuming different elastic foundation parameters. An increased thickness ratio L/h leads to a monotone reduction of the buckling load, with a meaningful effect of the shear foundation parameter K_g on the buckling results.

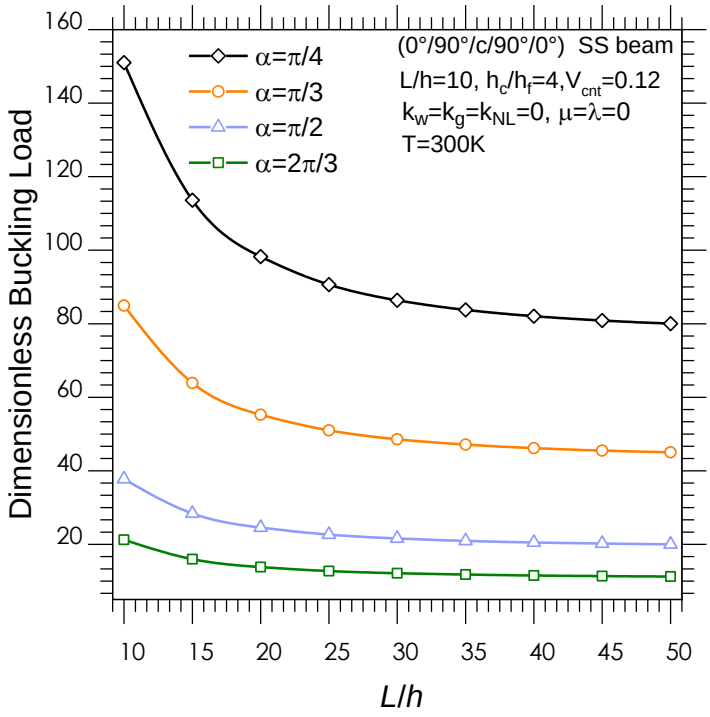

Figure 3. Dimensionless buckling load versus thickness ratio.

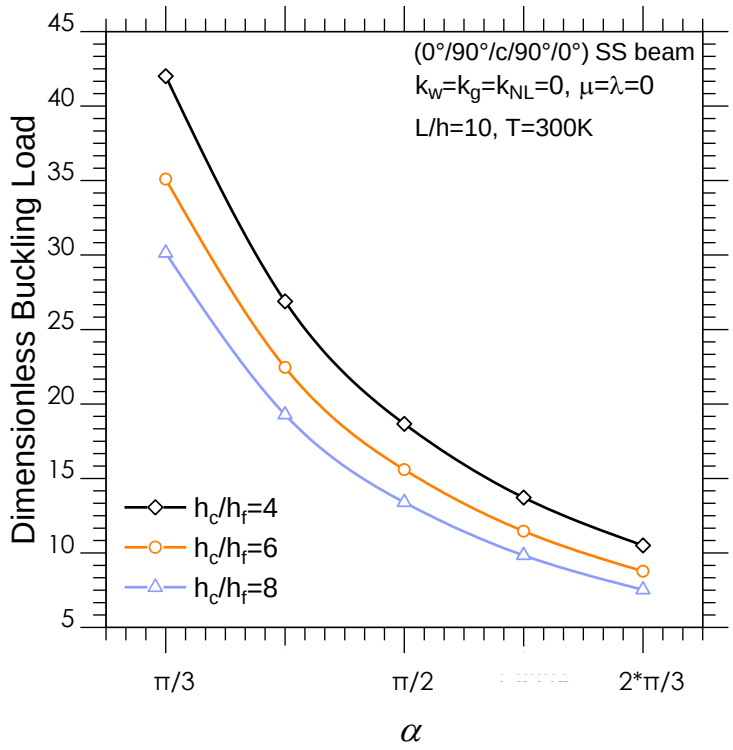

Figure 4. Dimensionless buckling load versus opening angle.

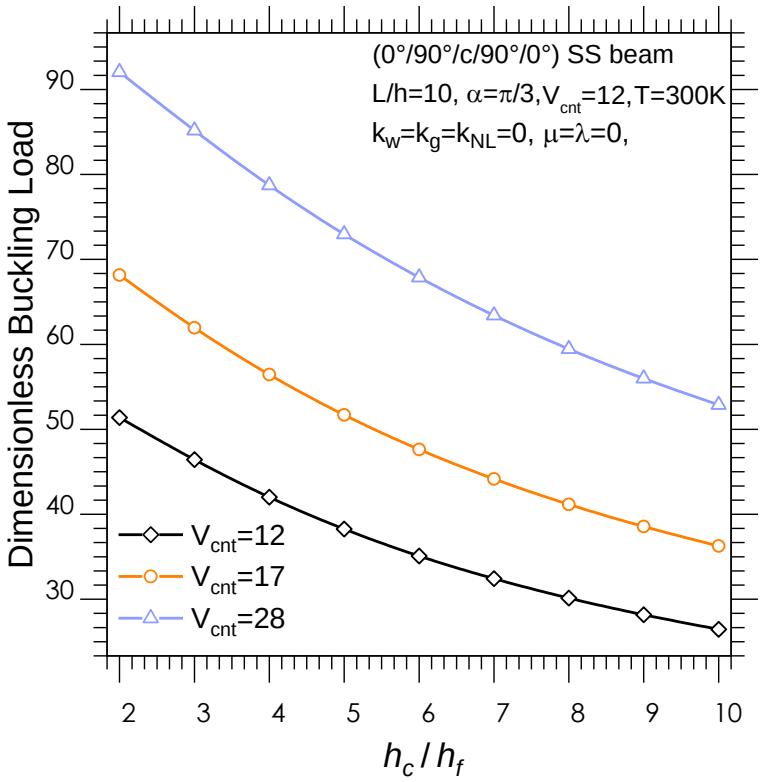

Figure 5. Dimensionless buckling load versus the core-to-face sheet thickness ratio.

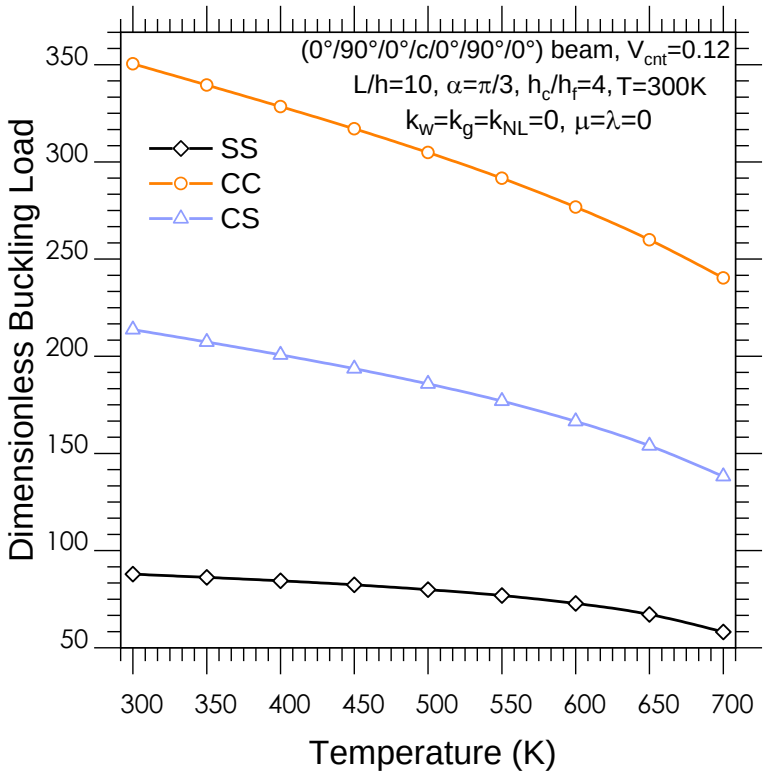

Figure 6. Dimensionless buckling load versus temperature.

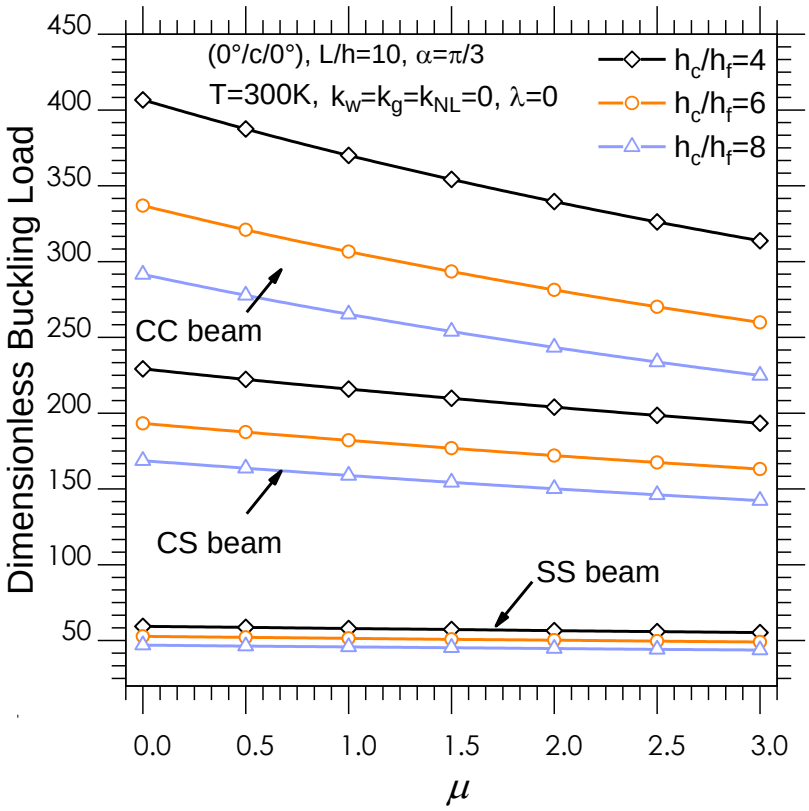

Figure 7. Dimensionless buckling load versus the nonlocal parameter.

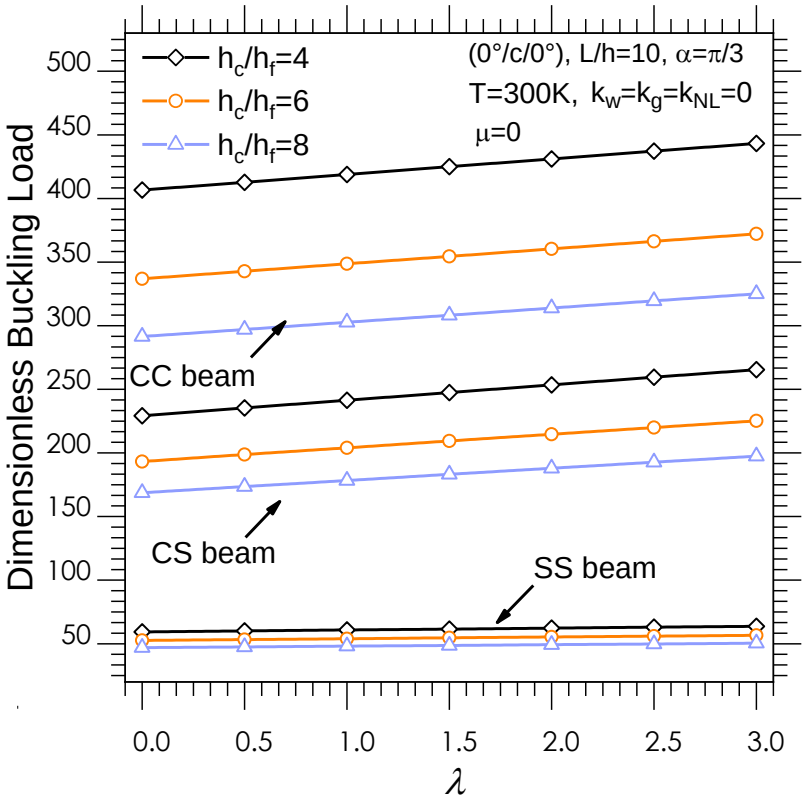

Figure 8. Dimensionless buckling load versus the length scale parameter.

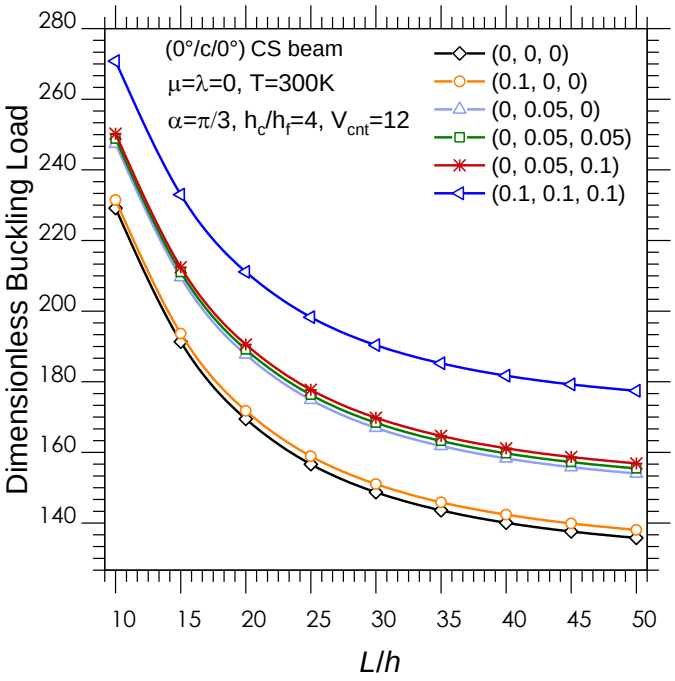

Figure 9. Effect of thickness ratio and elastic foundation on the dimensionless buckling load.

6. Conclusions

A novel quasi-3D higher-order shear deformation theory was proposed in this work to study the buckling response of CNTRC curved sandwich nanobeams for the first time. The problem was tackled theoretically, based on a Galerkin procedure, accounting for different boundary conditions and size-dependent effects. The material properties of CNTRC sheets were here assumed to be temperature-dependent, in agreement with the Touloukian principle.

A parametric study was performed systematically, to check for the influence of some significant parameters on the buckling response of CNTRC curved sandwich nanobeams, namely the CNTs reinforcement patterns and the nonlocal and length scale parameter, together with the geometric parameters. Based on the parametric investigation, it seems that the critical buckling load decreases for an increased temperature because of a global reduction in the stiffness of CNTRC curved sandwich nanobeams. Possible size effects can reduce the overall stiffness of CNTRC curved sandwich nanobeams, whereby the dimensionless critical buckling load decreases for an increased nonlocal parameter μ. Unlike the nonlocality effect, an increased length scale parameter λ leads to an increased buckling stability. More flexible elastic foundations and boundary conditions can reduce significantly the overall structural stability, which is also largely affected by a varying core-to-face sheet thickness ratio h_c/h_f, opening angle α, and CNT volume fractions. The results obtained by neglecting the effect of thickness stretching $(\varepsilon = 0)$ are perfectly in line with predictions from the literature, thus confirming the good accuracy of the proposed method to handle similar problems. The results obtained in this work, could represent valid benchmarks for engineers and researchers to validate different numerical methods as well as for practical design purposes of nanostructures.

Author Contributions: Conceptualization, A.A.D., M.S.A.H., B.K., R.D. and F.T.; Data curation, A.A.D. and B.K.; Formal analysis, M.S.A.H., B.K., R.D. and F.T.; Investigation, A.A.D., R.D. and F.T.; Methodology, M.S.A.H., M.A.E., R.D. and F.T.; Supervision, R.D. and F.T.; Validation, A.A.D., B.K., M.A.E., R.D. and F.T.; Writing—original draft, A.A.D., M.S.A.H., B.K. and M.A.E.; Writing—review & editing, R.D. and F.T. All authors have read and agreed to the published version of the manuscript.

Funding: This research receive no funding.

Conflicts of Interest: The authors declare no conflict of interest.

References

1. Griebel, M.; Hamaekers, J. Molecular dynamics simulations of the elastic moduli of polymer–carbon nanotube composites. *Comput. Methods Appl. Mech. Eng.* **2004**, *193*, 1773–1788. [CrossRef]
2. Han, Y.; Elliott, J. Molecular dynamics simulations of the elastic properties of polymer/carbon nanotube composites. *Comput. Mater. Sci.* **2007**, *39*, 315–323. [CrossRef]
3. Fidelus, J.; Wiesel, E.; Gojny, F.; Schulte, K.; Wagner, H. Thermo-mechanical properties of randomly oriented carbon/epoxy nanocomposites. *Compos. Part A Appl. Sci. Manuf.* **2005**, *36*, 1555–1561. [CrossRef]
4. Shen, H.-S. Nonlinear bending of functionally graded carbon nanotube-reinforced composite plates in thermal environments. *Compos. Struct.* **2009**, *91*, 9–19. [CrossRef]
5. Lim, C.; Zhang, G.; Reddy, J. A higher-order nonlocal elasticity and strain gradient theory and its applications in wave propagation. *J. Mech. Phys. Solids* **2015**, *78*, 298–313. [CrossRef]
6. Wu, H.; Kitipornchai, S.; Yang, J. Free Vibration and Buckling Analysis of Sandwich Beams with Functionally Graded Carbon Nanotube-Reinforced Composite Face Sheets. *Int. J. Struct. Stab. Dyn.* **2015**, *15*, 1540011. [CrossRef]
7. Eltaher, M.; Khater, M.; Park, S.; Abdel-Rahman, E.; Yavuz, M. On the static stability of nonlocal nanobeams using higher-order beam theories. *Adv. Nano Res.* **2016**, *4*, 51–64. [CrossRef]
8. Ebrahimi, F.; Farazmandnia, N. Vibration analysis of functionally graded carbon nanotube-reinforced composite sandwich beams in thermal environment. *Adv. Aircr. Spacecr. Sci.* **2018**, *5*, 107. [CrossRef]
9. Sobhy, M.; Zenkour, A.M. Magnetic field effect on thermomechanical buckling and vibration of viscoelastic sandwich nanobeams with CNT reinforced face sheets on a viscoelastic substrate. *Compos. Part B Eng.* **2018**, *154*, 492–506. [CrossRef]
10. Daikh, A.A.; Megueni, A. Thermal buckling analysis of functionally graded sandwich plates. *J. Therm. Stress.* **2018**, *41*, 139–159. [CrossRef]
11. Arefi, M.; Arani, A.H.S. Higher order shear deformation bending results of a magnetoelectrothermoelastic functionally graded nanobeam in thermal, mechanical, electrical, and magnetic environments. *Mech. Based Des. Struct. Mach.* **2018**, *46*, 669–692. [CrossRef]
12. Bekhadda, A.; Cheikh, A.; Bensaid, I.; Hadjoui, A.; Daikh, A.A. A novel first order refined shear-deformation beam theory for vibration and buckling analysis of continuously graded beams. *Adv. Aircr. Spacecr. Sci.* **2019**, *6*, 189–206. [CrossRef]
13. Medani, M.; Benahmed, A.; Zidour, M.; Heireche, H.; Tounsi, A.; Bousahla, A.A.; Tounsi, A.; Mahmoud, S.R. Static and dynamic behavior of (FG-CNT) reinforced porous sandwich plate using energy principle. *Steel Compos. Struct.* **2019**, *32*, 595–610. [CrossRef]
14. Arani, A.G.; Pourjamshidian, M.; Arefi, M.; Arani, M.R. Thermal, electrical and mechanical buckling loads of sandwich nanobeams made of FG-CNTRC resting on Pasternak's foundation based on higher order shear deformation theory. *Struct. Eng. Mech.* **2019**, *69*, 439–455. [CrossRef]
15. Nejati, M.; Ghasemi-Ghalebahman, A.; Soltanimaleki, A.; Dimitri, R.; Tornabene, F. Thermal vibration analysis of SMA hybrid composite double curved sandwich panels. *Compos. Struct.* **2019**, *224*, 111035. [CrossRef]
16. Chaht, F.L.; Kaci, A.; Houari, M.S.A.; Tounsi, A.; Beg, O.A.; Mahmoud, S. Bending and buckling analyses of functionally graded material (FGM) size-dependent nanoscale beams including the thickness stretching effect. *Steel Compos. Struct.* **2015**, *18*, 425–442. [CrossRef]
17. Ahouel, M.; Houari, M.S.A.; Bedia, E.A.; Tounsi, A. Size-dependent mechanical behavior of functionally graded trigonometric shear deformable nanobeams including neutral surface position concept. *Steel Compos. Struct.* **2016**, *20*, 963–981. [CrossRef]
18. Bouafia, K.; Kaci, A.; Houari, M.S.A.; Benzair, A.; Tounsi, A. A nonlocal quasi-3D theory for bending and free flexural vibration behaviors of functionally graded nanobeams. *Smart Struct. Syst.* **2017**, *19*, 115–126. [CrossRef]
19. She, G.-L.; Jiang, X.Y.; Karami, B. On thermal snap-buckling of FG curved nanobeams. *Mater. Res. Express* **2019**, *6*, 115008. [CrossRef]
20. She, G.-L.; Yuan, F.-G.; Karami, B.; Ren, Y.-R.; Xiao, W.-S. On nonlinear bending behavior of FG porous curved nanotubes. *Int. J. Eng. Sci.* **2019**, *135*, 58–74. [CrossRef]
21. Daikh, A.A.; Houari, M.S.A.; Tounsi, A. Buckling analysis of porous FGM sandwich nanoplates due to heat conduction via nonlocal strain gradient theory. *Eng. Res. Express* **2019**, *1*, 015022. [CrossRef]
22. Daikh, A.A.; Bachiri, A.; Houari, M.S.A.; Tounsi, A. Size dependent free vibration and buckling of multilayered carbon nanotubes reinforced composite nanoplates in thermal environment. *Mech. Based Des. Struct. Mach.* **2020**, 1–29, in press. [CrossRef]
23. Daikh, A.A.; Drai, A.; Bensaid, I.; Houari, M.S.A.; Tounsi, A. On vibration of functionally graded sandwich nanoplates in the thermal environment. *J. Sandw. Struct. Mater.* **2020**, 1–28, in press. [CrossRef]
24. Daikh, A.A.; Guerroudj, M.; El Adjrami, M.; Megueni, A. Thermal Buckling of Functionally Graded Sandwich Beams. *Adv. Mater. Res.* **2019**, *1156*, 43–59. [CrossRef]
25. Eltaher, M.; Mohamed, S.; Melaibari, A. Static stability of a unified composite beams under varying axial loads. *Thin-Walled Struct.* **2020**, *147*, 106488. [CrossRef]
26. Hamed, M.A.; Abo-Bakr, R.M.; Mohamed, S.A.; Eltaher, M.A. Influence of axial load function and optimization on static stability of sandwich functionally graded beams with porous core. *Eng. Comput.* **2020**, *36*, 1929–1946. [CrossRef]

27. Melaibari, A.; Abo-Bakr, R.M.; Mohamed, S.; Eltaher, M. Static stability of higher order functionally graded beam under variable axial load. *Alex. Eng. J.* **2020**, *59*, 1661–1675. [CrossRef]
28. Zenkour, A.M.; Daikh, A.A. Bending of functionally graded sandwich nanoplates resting on Pasternak foundation under different boundary conditions. *J. Appl. Comput. Mech.* **2020**, *6*, 1245–1259. [CrossRef]
29. Senturia, S.D. *Microsystem Design*; Springer Science & Business Media: Berlin, Germany, 2007.
30. Emam, S.A.; Eltaher, M.A.; Khater, M.E.; Abdalla, W.S. Postbuckling and Free Vibration of Multilayer Imperfect Nanobeams under a Pre-Stress Load. *Appl. Sci.* **2018**, *8*, 2238. [CrossRef]
31. Shi, D.-L.; Feng, X.-Q.; Huang, Y.Y.; Hwang, K.-C.; Gao, H. The Effect of Nanotube Waviness and Agglomeration on the Elastic Property of Carbon Nanotube-Reinforced Composites. *J. Eng. Mater. Technol.* **2004**, *126*, 250–257. [CrossRef]
32. Khater, M.; Eltaher, M.; Abdel-Rahman, E.; Yavuz, M. Surface and thermal load effects on the buckling of curved nanowires. *Eng. Sci. Technol. Int. J.* **2014**, *17*, 279–283. [CrossRef]
33. Brischetto, S.; Tornabene, F. Advanced GDQ models and 3D stress recovery in multilayered plates, spherical and double-curved panels subjected to transverse shear loads. *Compos. Part B Eng.* **2018**, *146*, 244–269. [CrossRef]
34. Tornabene, F.; Bacciocchi, M. Dynamic stability of doubly-curved multilayered shells subjected to arbitrarily oriented angular velocities: Numerical evaluation of the critical speed. *Compos. Struct.* **2018**, *201*, 1031–1055. [CrossRef]
35. Tornabene, F. On the critical speed evaluation of arbitrarily oriented rotating doubly-curved shells made of functionally graded materials. *Thin-Walled Struct.* **2019**, *140*, 85–98. [CrossRef]
36. Mohamed, N.; Eltaher, M.; Mohamed, S.; Seddek, L. Numerical analysis of nonlinear free and forced vibrations of buckled curved beams resting on nonlinear elastic foundations. *Int. J. Non-Linear Mech.* **2018**, *101*, 157–173. [CrossRef]
37. Karami, B.; Janghorban, M.; Tounsi, A. Variational approach for wave dispersion in anisotropic doubly-curved nanoshells based on a new nonlocal strain gradient higher order shell theory. *Thin-Walled Struct.* **2018**, *129*, 251–264. [CrossRef]
38. Arefi, M.; Pourjamshidian, M.; Arani, A.G. Free vibration analysis of a piezoelectric curved sandwich nano-beam with FG-CNTRCs face-sheets based on various high-order shear deformation and nonlocal elasticity theories. *Eur. Phys. J. Plus* **2018**, *133*, 193. [CrossRef]
39. Arefi, M.; Bidgoli, E.M.-R.; Dimitri, R.; Tornabene, F.; Reddy, J.N. Size-Dependent Free Vibrations of FG Polymer Composite Curved Nanobeams Reinforced with Graphene Nanoplatelets Resting on Pasternak Foundations. *Appl. Sci.* **2019**, *9*, 1580. [CrossRef]
40. Karami, B.; Janghorban, M.; Shahsavari, D.; Dimitri, R.; Tornabene, F. Nonlocal Buckling Analysis of Composite Curved Beams Reinforced with Functionally Graded Carbon Nanotubes. *Molecules* **2019**, *24*, 2750. [CrossRef]
41. Karami, B.; Shahsavari, D.; Janghorban, M.; Li, L. Influence of homogenization schemes on vibration of functionally graded curved microbeams. *Compos. Struct.* **2019**, *216*, 67–79. [CrossRef]
42. Arefi, M.; Bidgoli, E.M.-R.; Dimitri, R.; Bacciocchi, M.; Tornabene, F. Nonlocal bending analysis of curved nanobeams reinforced by graphene nanoplatelets. *Compos. Part B Eng.* **2019**, *166*, 1–12. [CrossRef]
43. Eltaher, M.; Mohamed, N.; Mohamed, S.; Seddek, L. Periodic and nonperiodic modes of postbuckling and nonlinear vibration of beams attached to nonlinear foundations. *Appl. Math. Model.* **2019**, *75*, 414–445. [CrossRef]
44. Malikan, M.; Nguyen, V.B.; Dimitri, R.; Tornabene, F. Dynamic modeling of non-cylindrical curved viscoelastic single-walled carbon nanotubes based on the second gradient theory. *Mater. Res. Express* **2019**, *6*, 075041. [CrossRef]
45. Mohamed, N.; Eltaher, M.A.; Mohamed, S.A.; Seddek, L.F. Energy equivalent model in analysis of postbuckling of imperfect carbon nanotubes resting on nonlinear elastic foundation. *Struct. Eng. Mech.* **2019**, *70*, 737–750. [CrossRef]
46. Van Tham, V.; Quoc, T.H.; Tu, T.M. Free Vibration Analysis of Laminated Functionally Graded Carbon Nanotube-Reinforced Composite Doubly Curved Shallow Shell Panels Using a New Four-Variable Refined Theory. *J. Compos. Sci.* **2019**, *3*, 104. [CrossRef]
47. Dindarloo, M.H.; Li, L.; Dimitri, R.; Tornabene, F. Nonlocal Elasticity Response of Doubly-Curved Nanoshells. *Symmetry* **2020**, *12*, 466. [CrossRef]
48. Eltaher, M.A.; Mohamed, N. Nonlinear stability and vibration of imperfect CNTs by Doublet mechanics. *Appl. Math. Comput.* **2020**, *382*, 125311. [CrossRef]
49. Karami, B.; Shahsavari, D. On the forced resonant vibration analysis of functionally graded polymer composite doubly-curved nanoshells reinforced with graphene-nanoplatelets. *Comput. Methods Appl. Mech. Eng.* **2020**, *359*, 112767. [CrossRef]
50. Karami, B.; Janghorban, M.; Tounsi, A. Novel study on functionally graded anisotropic doubly curved nanoshells. *Eur. Phys. J. Plus* **2020**, *135*, 103. [CrossRef]
51. Mohamed, N.; Mohamed, S.A.; Eltaher, M.A. Buckling and post-buckling behaviors of higher order carbon nanotubes using energy-equivalent model. *Eng. Comput.* **2020**, 1–14, in press. [CrossRef]
52. Eringen, A.C. On differential equations of nonlocal elasticity and solutions of screw dislocation and surface waves. *J. Appl. Phys.* **1983**, *54*, 4703–4710. [CrossRef]
53. Touloukian, Y.S. *Thermophysical Properties of High Temperature Solid Materials*; MacMillan: New York, NY, USA, 1967.